PCCP

PAPER

View Article Online
View Journal | View Issue

Cite this: *Phys. Chem. Chem. Phys.*, 2017, **19**, 6757

The dynamic conductance response and mechanics-modulated memristive behavior of the Azurin monolayer under cyclic loads†

Xiaoyue Zhang,[abc] Jian Shao,[ab] Yun Chen,[ab] Weijin Chen,[abc] Jing Yu,[ab] Biao Wang[ac] and Yue Zheng*[abd]

Received 24th November 2016,
Accepted 1st February 2017

DOI: 10.1039/c6cp08044h

rsc.li/pccp

Azurin (Az) has been considered as the research hotspot in molecular electronics, as well as a promising material for building functional devices on the molecular scale because of its special electrical properties and force-dependent conductance effects. Here we carry out an in-depth investigation combined with molecular scale experiments, molecular dynamics simulations, first-principles calculations and theoretical models to reveal the dynamic conductance response of the Az monolayer under cyclic mechanical loading. Experimentally, the conductance of the Az monolayer under continuous cyclic loads was recorded using a conductive atomic force microscope. Our results demonstrate the strong nonlinear force-dependence and significant time-delayed characteristics, which distinctly differ from the results obtained under stepwise loading. It is also found that the period and amplitude of cyclic loads have a great impact on the magnitude, peak value and change rate of the current. The regular dynamic response of the Az conductance under mechanical force looks like a type of memristive behavior, which is defined as mechanics-modulated memristive behavior in this work. In order to verify these peculiar experimental results, we employed both molecular dynamics simulations and first-principles calculations to analyze the structural deformation and molecular orbitals of Az under cyclic loads. A phenomenological model is also established to explain experimental findings and further illustrate mechanics-modulated memristive behavior.

Introduction

The idea of using single molecules or molecular monolayers to build electronic devices has attracted extensive attention due to their natural advantages such as extremely small size, sensitivity to external signals, tolerance to large deformation and so on.[1–4] Among the numerous chemical compounds, bio-macromolecules such as proteins are often considered as promising candidates because of the intimate connection between their delicate molecular structure and electric properties.[5–7] On one hand, the variety of chemical moieties and bonds in macromolecules provide numerous building blocks for constructing functional molecular devices with novel electrical properties, including rectification,[8] negative differential resistance[9] and even ferroelectric behavior,[10,11] *etc.* More importantly, the structure of macromolecules is exquisitely susceptible to external stimuli such as mechanical force, pH, temperature as well as specific bindings and enzyme catalysis.[12,13] Thus molecular devices constituted of macromolecules are promising in achieving high controllability, sensitivity and selectivity,[14,15] *etc.* While tremendous works have been dedicated to explore the mechanism and applications of macromolecule-based molecular devices,[16–19] we are especially interested in the force modulation of protein conductance. Mechanical load can easily affect the protein structure in the most direct way, thus it has an inevitable effect on electron transport and thereby is critical to the performance of protein-based molecular devices. Besides, electron transport of proteins is involved in many bio-processes such as adenosine triphosphate production and photosynthesis.[20] Thus comprehensive understanding of the force effect on electron transport in proteins might bring new thoughts to some important biological issues such as mechano-transduction and mechanical signaling.[21,22]

Azurin (Az), an electron-mediating protein from bacteria, is one of the research focuses in molecular electronics because

[a] *State Key Laboratory of Optoelectronic Materials and Technologies, Sun Yat-sen University, Guangzhou, 510275, China. E-mail: zhengy35@mail.sysu.edu.cn*
[b] *Micro&Nano Physics and Mechanics Research Laboratory, School of Physics, Sun Yat-sen University, Guangzhou, 510275, China*
[c] *Sino-French Institute of Nuclear Engineering and Technology, Sun Yat-sen University, Zhuhai, 519082, China*
[d] *Departments of Mechanical Engineering and Civil and Environmental Engineering, Northwestern University, Evanston, IL 60208, USA*

† Electronic supplementary information (ESI) available. See DOI: 10.1039/c6cp08044h

of its special electrical properties and force-dependent conductance effects.[23–26] By using a conductive atomic force microscope (CAFM), previous studies have shown that the conductance of the Az monolayer increases in proportion to the tip force on the sample, and remains unchanged during the decrease of force. Thereby, the hysteresis effect of the conductance appears during loading and unloading processes.[23] Such an electronic response to mechanical force is interesting and important, which endows Az with great potential for building functional devices. However, all previous studies investigated this issue by obtaining *I–V* spectra only under stepwise loading, and the response of the conductance on the mechanical load is static or at least quasi-static. As a result, the dynamic response of Az conductance on the load is hidden, unrevealed and an important issue urged for an in-depth study. Davis *et al.*[25] have suggested that the plasticity should be the origin of conductance hysteresis. Thus it is a reasonable association that the possible dynamic characteristics of proteins, such as viscoelasticity and viscoplasticity, could dominate the dynamic response of Az conductance. In this scenario, the time integral of force on the sample should play the key role in producing deformation, structural changes and thereby the conductance variation in Az. Owing to such a force-dependent conductance exhibiting process-related characteristic and showing the dynamic history, Az might well show a type of memristive behavior.[27–31] Recently, memristive systems have attracted extensive attention and have been deemed to have revolutionary values for non-volatile information storage, research for adaptation and even learning behavior. In this regard, the underlying force-dependent memristive behavior of Az should also be of much scientific importance and application prospect.

In this paper, we define the dynamic response of Az conductance on the mechanical force as mechanical-modulated memristive (MMM) behavior, and conducted a comprehensive study on the dynamic conductance response and the MMM behavior of the Az monolayer under cyclic loads. Experimentally, the conductance of the Az monolayer under both quasi-static and dynamic cyclic loads was recorded and analyzed using CAFM. The dynamic conductance response and MMM behavior of Az were revealed. In order to verify these experimental results, combined molecular dynamics simulations and first-principles approaches were carried out to explore the origin of MMM behavior. A theoretical model has also been established to describe the dynamic conductance response and MMM behavior and explain our view towards the influence of the force on the electron transport of proteins.

Experimental and simulations

Az monolayer preparation and CAFM measurements

The Az monolayer was prepared by directly immobilizing the proteins on an atomic flat Au substrate (see Fig. S1, ESI†), utilizing the surface disulfide bridge between Cys3 and Cys26. 1 mg of Az lyophilized powder from *Pseudomonas aeruginosa* (Sigma A3672) was first mixed with 1 ml of ultrapure water to form a 5 μM solution in acetate buffer. An atomic flat Au substrate (Fig. S1, ESI†) prepared by hydrogen flame annealing was then immersed in the solution for at least 2 hours, followed by thorough rinsing with ultrapure water (18.2 MΩ) and blow drying with nitrogen before the measurements. All CAFM measurements were performed using a CSPM 5500 (Being Co. Ltd). Morphology mapping was obtained in a tapping mode using a tip with a force constant of 45 N m^{-1} and a frequency of ~300 kHz. The thickness of the monolayer was acquired by means of the scrape test, in which 5 × 5 μm of the monolayer was first scraped from the substrate in a contact mode. As a result, the profile of the Az monolayer was exposed at the boundary of the scraped area. The morphology and the section line of the cliff were then obtained in a tapping mode.

Molecular dynamics simulations and molecular orbital calculations

While modeling the structure of Azurin, protein data bank (PDB) entries 4AZU from *Pseudomonas aeruginosa* and 1JOI from *Pseudomonas fluorescens* are both typical and widely used in various studies.[32,33] These two PDB entries show almost the same structure. In the simulations, 4AZU is usually operated using the Gromos force field, and 1JOI can be simulated using the CHARMM22 force field, which handles the Cu-centered metal–ligand complex more precisely and is essential for our following orbital analysis.[34] In order to precisely analyse the effect of the mechanical loads on the conductance of the Azurin monolayer, we carried out the molecular dynamics simulations using the CHARMM22 force field.[35] The Cu-centered metal–ligand complex was modeled with the parameters from the study of Ungar L. *et al.*[36] To take into account the mechanical effects of the electrodes, the substrate and the tip were represented by the (111) surface of the Au substrate with 6.9 × 8.0 nm^2 area and 6-atomic-layer thickness. The CHARMM-METAL intermolecular potential[37] was used to model both surfaces with 4608 atoms each. The time step for all simulations was 1 fs. The protein was first allowed to relax on the fixed substrate and then to equilibrium at 300 K. Meanwhile the distance between the centers of the tip and the substrate was used as the collective variable (CV) and was kept fixed in 6.0 nm. Then the tip was pushed towards the substrate and the CV was reduced from 6.0 nm to 3.2 nm at a speed of 4.0 m s^{-1}. During the process, the tip touched and subsequently squeezed the protein on the substrate. After that, the CV was cycled between 3.2 nm and 3.8 nm repeatedly at a speed of 0.3 m s^{-1} for three and half periods. For the protein, two snapshots during molecular dynamics simulations, where the force was 2 nN in the first cycle, were picked for density functional theory (DFT) calculations in the Atomistix ToolKit (ATK).[38] Perdew–Burke–Ernzerhof generalized gradient approximation (PBE-GGA)[39] was employed. A single-ζ polarized basis set with an energy cutoff of 75 Ry was used for all the atoms and self-consistency was achieved at 10^{-4} Ry.

Results and discussion

Morphology and thickness of the Az monolayer

To verify the preparation of the samples, we first examined their morphology *via* AFM in tapping mode. As shown in Fig. 1a,

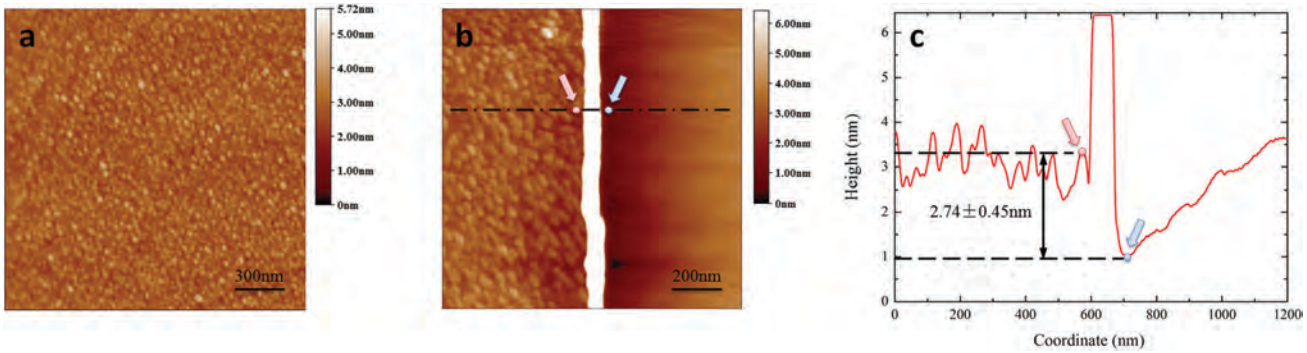

Fig. 1 (a) Typical AFM image of the Az monolayer prepared on the Au substrate. (b) AFM image of the Az monolayer after the scraping test. All Az was scraped off on the right part of the image, exposing the naked Au substrate. The morphology data extracted are indicated by the dashed line and plotted as the cross-section line shown in (c). The thickness of the monolayer is between 2 and 3 nm.

the typical morphology of Az monolayers has uniform surfaces with fluctuations less than 1 nm. The thickness of the monolayer was then checked carefully by means of scraping tests, where Az molecules were swept away from the chosen area by the AFM tip to expose the profile of the Az monolayer. Fig. 1b shows the typical AFM image of the Az monolayer after the scraping test, in which the cross-section corresponding to the dashed line has been illustrated in Fig. 1c. The peak in the middle of Fig. 1b and c was formed by molecular accumulation during the sweeping manipulation, which is irrelevant to the thickness estimation. The thickness of the Az monolayer was obtained by measuring the vertical drop between the upper surface of the Az film and the Au substrate, the edges of which have been pointed out with red and blue dots, respectively. Our result shows that the thickness of the Az monolayer was 2.74 ± 0.45 nm, which confirms that there was only one layer of molecules on the substrate.

The quasi-static response of Az conductance under cyclic loads

To compare the conductance response under different loads, we first measured the *I–V* spectra of Az monolayers subjected to stepwise cyclic loads. The schematic diagram of the *I–V* tests is illustrated in Fig. 2a. By CAFM,[40,41] a gold coated pyramidal tip with a 20 nm curvature radius was pressed on the Az monolayer to form the Au–Az–Au junction. By controlling the setpoint value, the tip force was allowed to cycle between 9 nN and 40.5 nN in a stepwise manner. Meanwhile, *I–V* curves in each loading level were recorded to plot the loading and unloading *I–V* spectra as shown in Fig. 2b and c, respectively. As expected, the two *I–V* spectra show diverse characteristics. During the loading process, *I–V* curves distribute evenly in diagram, and their slopes are highly in accordance with the force magnitude. However, in the unloading *I–V* spectrum, the distribution of *I–V* curves is obviously biased, in which most *I–V* curves retain large slopes even when the force is decreasing. To characterize the quasi-static force dependent resistance of the Az monolayer, we extracted the bias corresponding to 3.5 nA in each *I–V* curve as the nominal resistance for each loading level. As shown in Fig. 2d, the Az resistance exhibits obvious hysteresis behaviors under stepwise cyclic loads, which decreases almost linearly with the increase of force during the loading process, but tends to remain in the low resistance state during the unloading process from 40.5 nN to 27 nN. With a further decrease of force, the resistance of Az began to increase.

The dynamic response of Az conductance under cyclic loads

From the stepwise loading manner and the process for *I–V* tests, the quasi-static and discrete data might hide some important behavior, thereby concealing the dynamic response of the conductance on the mechanical load. To overcome these limitations, we adopted *I–Z* measurements to study the dynamic response of Az conductance under cyclic loads. In *I–Z* measurements, the input voltage for the vertical channel of the scanner (*i.e.* *Z* position) was controlled to cycle continuously between 0 V and 80 V with a period of 2000 ms. With the increase of the *Z* position (engaging), the scanner arises and thereby increases the pressing force subjected by the Az monolayer. Retreating is just the reverse. Meanwhile, 2 V bias was applied between the tip and the substrate, and the output current during both engaging and retreating was recorded and illustrated as a function of the *Z* position. The typical *I–Z* curve (solid line) is presented in Fig. 3. The force corresponding to the measurement (*i.e.* *F–Z* curve) is also shown with dashed lines. At the beginning of the measurement, the tip did not come into contact with the sample, and thus the probe cantilever was completely relaxed and no force was detected. The initial tip–sample contact occurred when the *Z* position reached $\sim$23 V, and the tip force increased linearly with the scanner ascending hereafter. However, the variation of current did not follow the linear regulation as quasi-static resistance hysteresis has suggested. Instead, the current was found to increase at an accelerating speed after the force exceeded $\sim$20 nN. With the maximum load of 70 nN, the current was 0.65 nA. More interestingly, when the tip force began to decrease from the maximum load, the current kept on increasing to 0.9 nA until the force was reduced to 60 nN. As a result, the peak current of the *I–Z* curve is located within the retreating range, which is in stark contrast to the quasi-static resistance hysteresis and becomes the most distinctive feature of the dynamic response of Az conductance under cyclic loads. This peculiar delayed peak current indicates that the change of

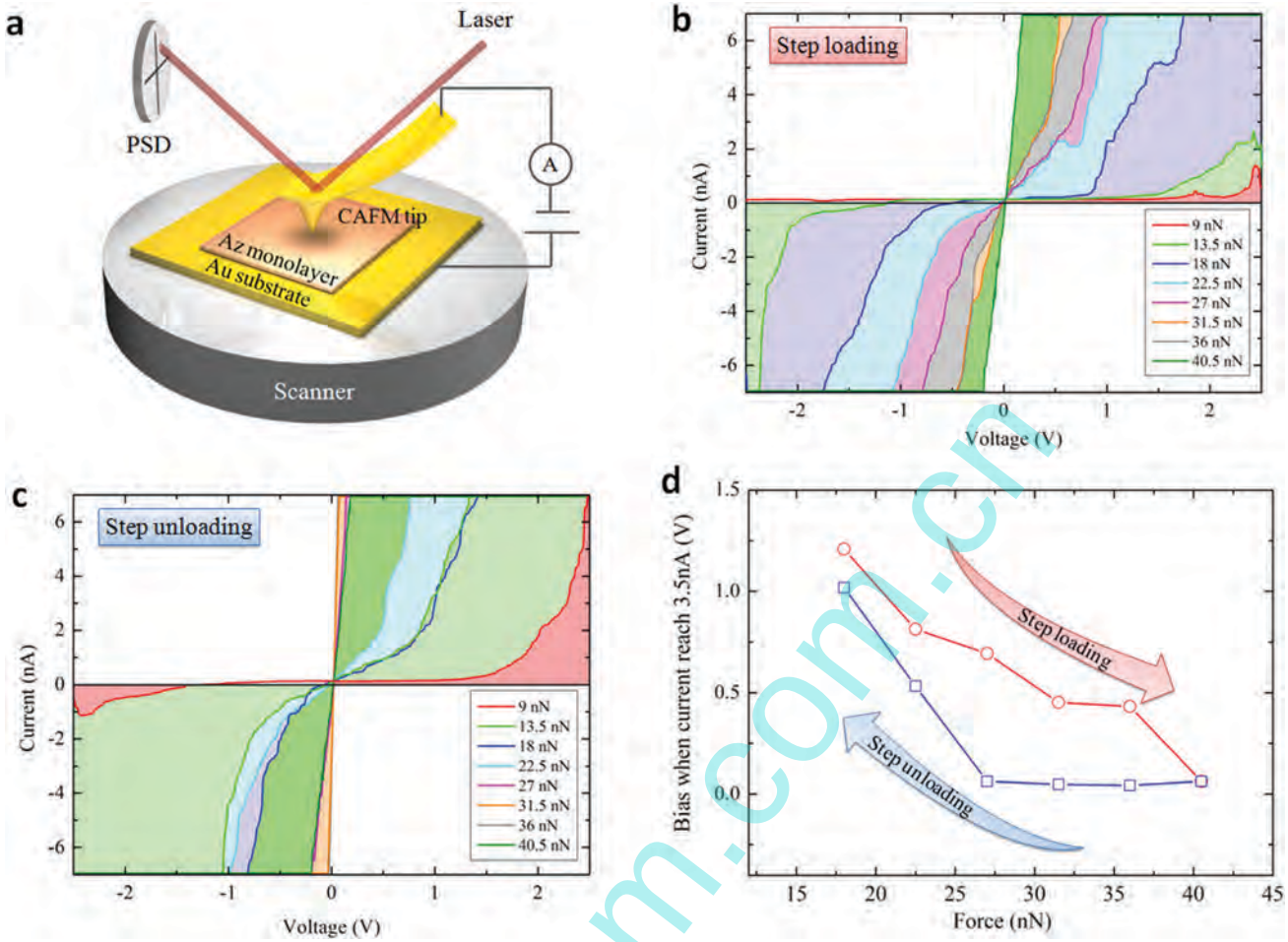

Fig. 2 (a) The schematic diagram of the *I*–*V* tests. (b) The loading *I*–*V* spectrum and (c) the unloading *I*–*V* spectrum. The difference between each loading level is 4.5 nN. (d) The resistance hysteresis extracted from *I*–*V* spectra. The bias when current reaches 3.5 nA of each *I*–*V* curve is considered as the nominal resistance.

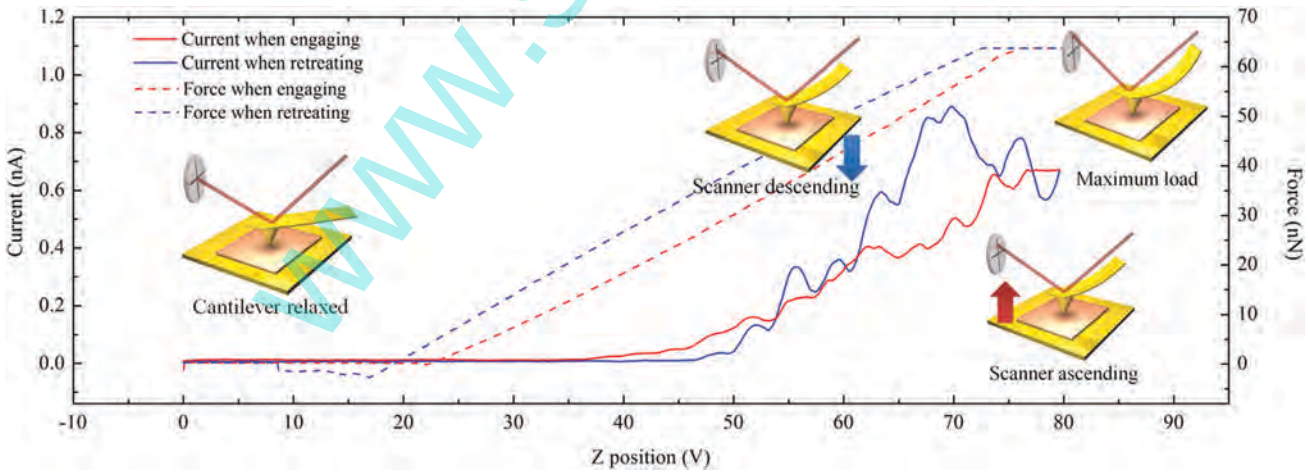

Fig. 3 The typical *I*–*Z* curve of the Az monolayer, in which red and blue solid lines represent the current during loading and unloading processes, respectively. And the magnitude of pressing force corresponding to the two processes is presented with red and blue dashed lines, respectively. In this measurement, the period of the cyclic load was 2000 ms, and the *z*-direction speed of the scanner was about 700 nm s^{-1}. It is remarkable to see that peak current appears during the retreating process.

the force-induced compression on the sample and molecular structures in the sample still increases the conductance even when the force began to decrease. Only after the force was smaller than a certain value, the conductance of the Az monolayer

began to decrease with the decrease of the force. In accordance with viscoelasticity, the deformation of Az is dominated by the time integral of force, and the conductance of Az should also be dependent on both the magnitude and the load rate of force. In fact, while the loading time in *I–Z* measurements (2 seconds per cycle) is shorter than that in *I–V* spectra (several minutes per cycle), the current obtained in *I–Z* measurements is obviously smaller than that in *I–V* spectra under 2 V.

To confirm and get deeper insight into the dynamic response of Az conductance, we further studied the influence of bias on the *I–Z* characteristic. A series of *I–Z* curves have been obtained and are shown in Fig. 4a–d. At the same time, by using a CAFM probe with a higher force constant (40 N m^{-1}), the peak force of cyclic load was increased to ~1100 nN (Fig. 4e) to amplify the phenomenon. Generally, all of the results in Fig. 4a–d confirm the observations in Fig. 3, and it is found that the delayed peak current is enhanced remarkably under the increased peak force. It is noteworthy that our results also indicate that bias has a non-negligible influence on the dynamic response of Az conductance. To characterize this influence, the ratios between maximum

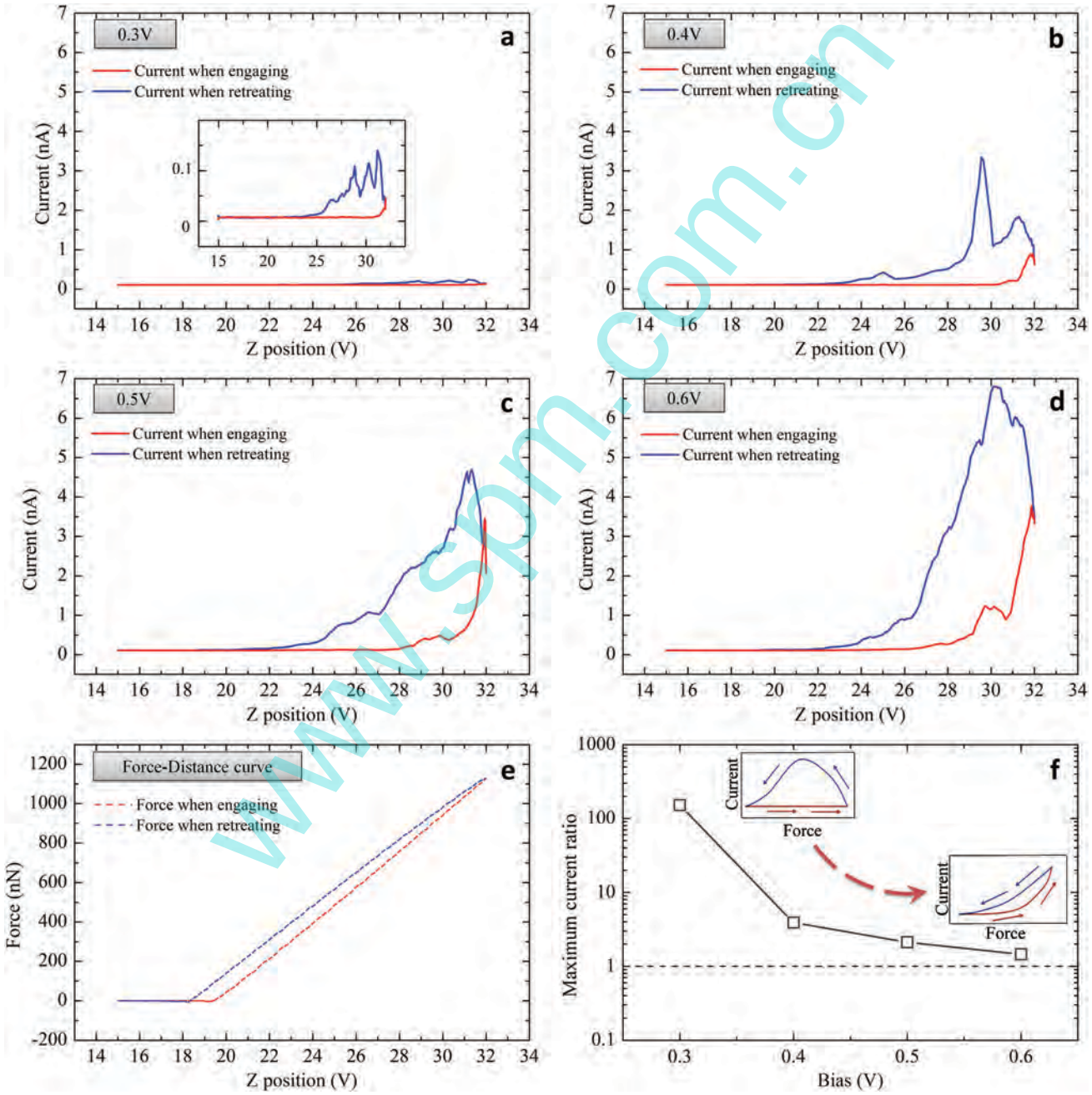

Fig. 4 (a–d) The *I–Z* curves obtained under 0.3 V (the inset shows detail of the *I–Z* curve with smaller current scale), 0.4 V, 0.5 V and 0.6 V bias, respectively. (e) The *F–Z* curves corresponding to the *I–Z* measurements. (f) The maximum current ratio as a function of bias, which shows a clear convergent tendency. The inset illustrates the characteristic of *I–Z* curves with different current ratio.

currents during retreating and engaging processes are plotted in Fig. 4f. As shown by the illustration, the maximum current ratio under 0.3 V is as high as 151. With the increase of bias, this ratio rapidly decreases and tends to approach 1. With a large ratio (>100), the *I–Z* characteristic will show a fully delayed current peak. However, if the ratio is reduced to 1, no delayed current peak can be observed. The *I–Z* measurements have been repeated on different samples and sites for hundreds of times. Most of the Az monolayers showed the characteristics of the nonlinear force-dependent conductance and delayed peak current except for some breakdown and undetectable samples. However, there are also fluctuations between data from different sites, which is probably induced by the uncertain contact between the tip and the monolayer.[40]

The time-domain response of Az conductance under cyclic loads

In order to make certain that the dynamic response of Az conductance is dominated by the time integral of force, we carried out further study on the time-domain response of Az conductance under cyclic loads. In this part of experiments, we replaced the pyramidal CAFM tip with a gold coat spherical tip (Novascan PT.GS.CONDUC), which has a curvature radius of 1 μm (Fig. S2, ESI†). According to the Hertz model,[27] the contact area between the monolayer and this spherical tip is at least 20 times larger than that with the pyramidal tip under the same force. Naturally, the current signal obtained with the spherical tip is contributed by more molecules and thereby more similar to the real situation in devices (Fig. 5a). Moreover, the pressure exerted by the monolayer is reduced accordingly, which should ensure that no undesired damage is caused to the substrate and the monolayer. Thus if the nonlinear force dependency and delayed peak current can still be observed with the spherical tip, it can be confirmed that the phenomena are not illusion. Using the spherical tip, we recorded the current variation of Az under cyclic loads as a function of time (*I–t* curve), and the typical results are shown in Fig. 5b. Four cycles of *I–t* curves were measured on the same site of the sample under 0.1 V bias. The peak force was increased after each cycle, and finally reached ~2400 nN in cycle iv (Fig. S3, ESI†). As we expected, all four cycles of *I–t* curves show exactly the same features as *I–Z* measurements with high-level consistency and reproducibility. Because of the low bias, current can only be observed at the end of engaging, which is in good agreement with the result in Fig. 4a. Hereafter, current accelerated with

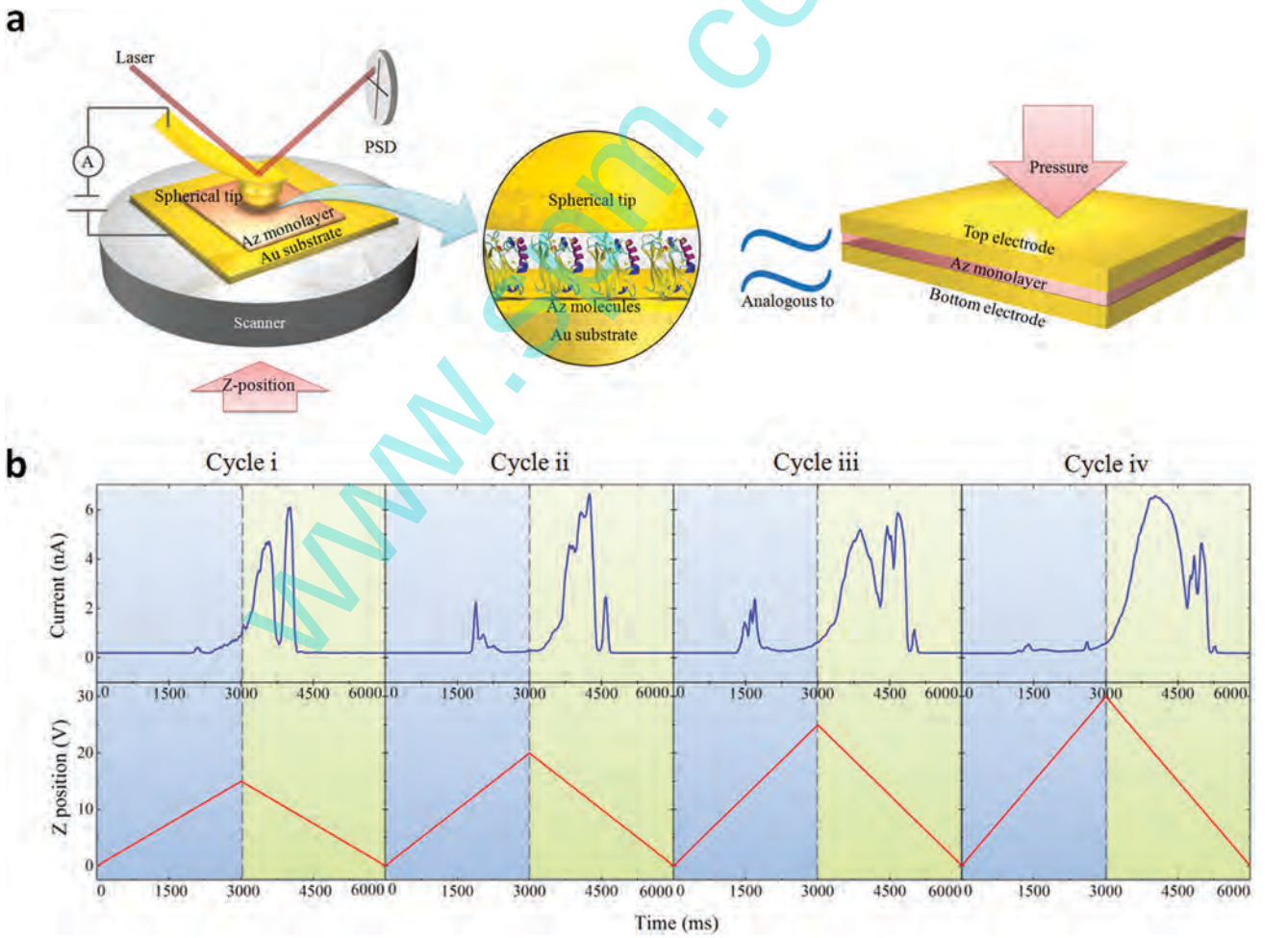

Fig. 5 (a) The schematic diagram for measuring current *vs.* time under cyclic loads with the spherical tip. (b) The *I–t* curves under cyclic loads. All the four cycles were obtained on the same site of the Az monolayer.

the ascending of the scanner. When the scanner began to descend, current kept on increasing, and formed the delayed peak currents. Multiple current peaks can be observed in all four cycles of *I–t* curves, which are probably caused by the morphology fluctuations of the Az monolayer. Among them, the first current peak in each retreating process increased with peak force. With 1200 nN peak force in cycle i, the value of the first delayed current peak is 4.8 nA, which increased to 6.7 nA in cycle iv with a peak force of 2400 nN. This result confirms that higher peak force leads to higher peak current. We also notice another remarkable phenomenon on the boundary of engaging and retreating that, although the time derivative of applied force is not continuous at this moment, no obvious turning point can be found in *I–t* curves. This time derivative continuity under triangular loads is consistent with our conjecture that Az conductance is affected by the time integral of force.

If it is true that the dynamic response of Az conductance under cyclic loads is dominated by the time integral of force, higher peak current should be observed under longer cyclic periods. To reveal this property, *I–t* curves with different cyclic periods have been measured. The typical results are plotted in Fig. 6, in which the four cycles were measured sequentially using the spherical tip under 0.7 V bias, and the peak force in all four cycles was in the same magnitude of 1022 nN. In cycles I and III with a period of 1000 ms, the maximum currents are about several hundred pA, which are one order of magnitude smaller than that in cycle II with a period of 5000 ms. In cycle IV with a period of 8000 ms, the maximum current is even higher, which exceeds the measuring range of our instrument. The above results clearly show that a longer load period will lead to higher peak current, which demonstrates the frequency dependency of Az conductance under cyclic loads. Such a property also explains the difference between *I–V* spectra in Fig. 2 and *I–Z* curves in Fig. 3. On the one hand, the stepwise load mode in measuring *I–V* spectra can be considered as a cyclic load with a very long period. Thus it is reasonable to see that current in *I–V* spectra is much higher than that in the *I–Z* curve under the same bias. On the other hand, the increase of Az conductance is certainly not unlimited. With a long time interval between each test, *I–V* spectra might only show the saturated current at each loading level. Consequently, no phenomenon like delayed peak current can be observed in resistance hysteresis.

The MMM behavior of Az

All our experimental results, including nonlinear force dependency, delayed peak current, time derivative continuity and period & peak force dependent peak current, indicate that Az conductance should be a function of time integral of force. To be specific, Az conductance $G(\lambda)$ can be considered to be determined by internal parameter λ, which reflects the structure-dependent factors that affect electron transport. While the applied force will cause deformation and structural change to Az, λ will certainly be altered accordingly. To simultaneously satisfy all the experimental results, the relationship between force F and λ should have the form $d\lambda/dt = f(F, \lambda)$, where $f(F, \lambda)$ is a nth order function of F ($n \geq 1$). Such a regulation aligns well with the basic mathematic of memristive systems.[29] Originally, the memristive system refers to a memristor, the resistance of which is dependent on the time integral of voltage or current. In recent years, this notion has been extended, and other types of mem-systems have been put forward, *e.g.* a charge-controlled memcapacitor and a current-controlled meminductive system. One distinguishing feature of all these mem-systems is that their electronic properties can be modulated continually by the flux of the controlling variable (*i.e.* time integral of voltage, charge or current). The mechanism can be attributed to the flux activated changes of the internal state such as ionic motion of oxygen vacancies, structure and phase transition. Here, since the conductance variation of the Az monolayer is activated by the time integral of mechanical force, we analogously define such a property as mechanics modulated memristive (MMM) behavior.

To further expound the MMM behavior of Az, we conducted a study combined with MD simulations[34–37] and first-principles calculations[42,43] to investigate the mechanical and electronic behaviors of the Az monolayer under cyclic loads. First, we carried out MD simulations to extract the mechanical and structural details of the Az molecule under cyclic loads. As shown in Fig. 7a, an Az molecule was placed between two Au electrodes with a

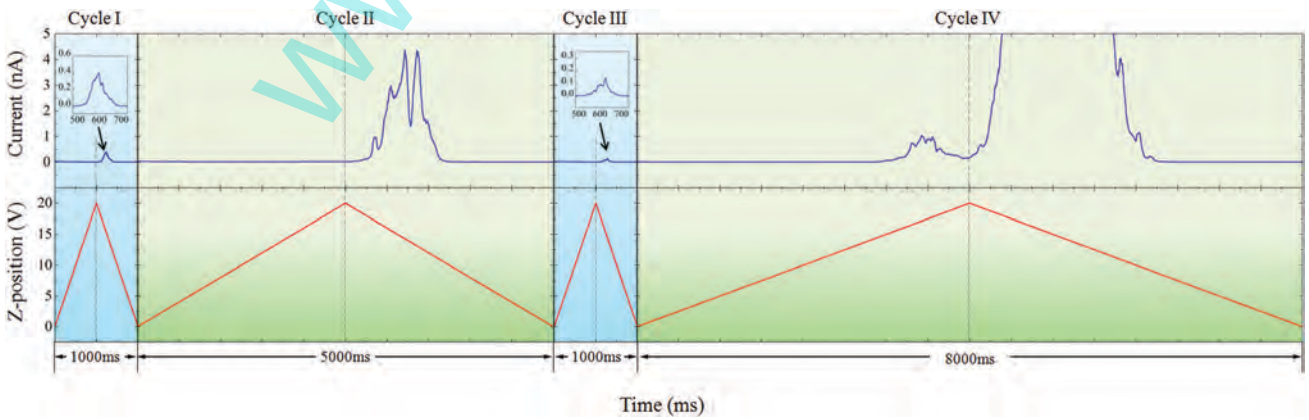

Fig. 6 The *I–t* curves under cyclic loads with different periods, here the load period of cycles I and III is 1000 ms; the load periods of cycle II and cycle IV are 5000 ms and 8000 ms, respectively.

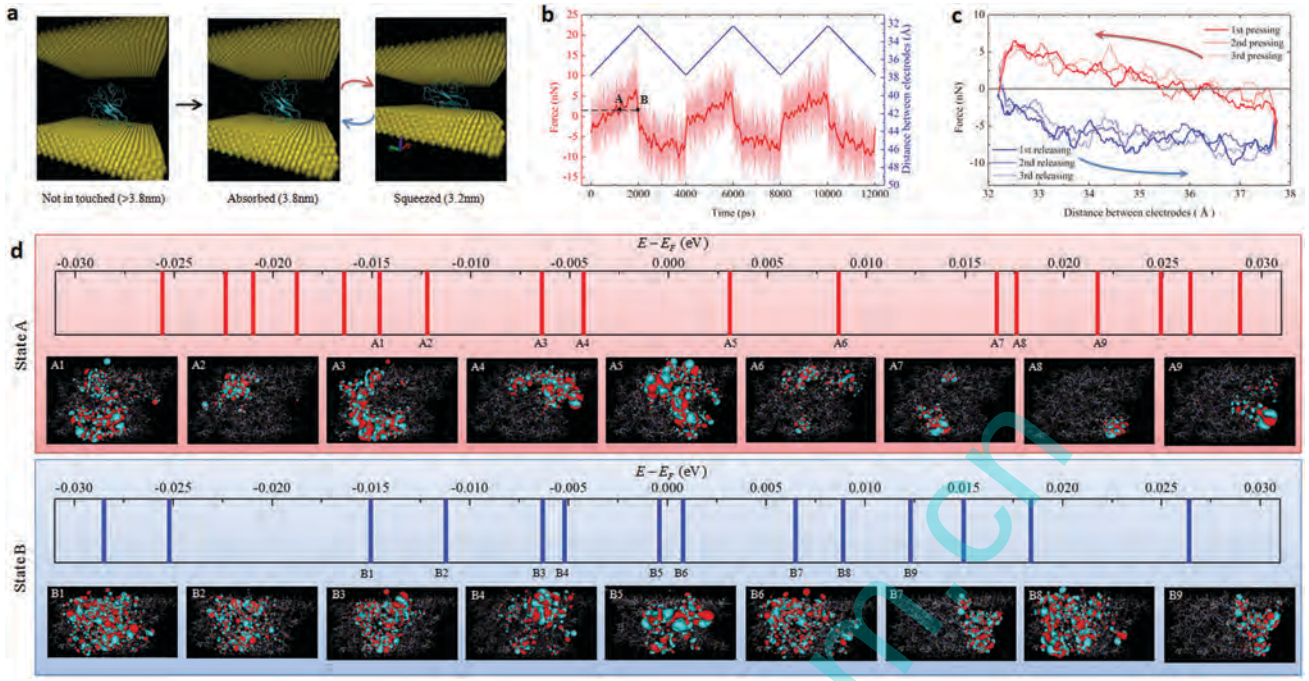

Fig. 7 (a) The snapshots of MD simulations with different distances between electrodes (6 nm, 3.8 nm, and 3.2 nm). (b) The force exerted on Az as a function of time and (c) distance between electrodes. (d) The energy spectra and isopotential surfaces of 9 orbitals that are near the Fermi level for both states A and B, where E is the energy level of the orbital and E_F is the Fermi level.

6-atomic-layer thickness at 300 K. After the molecule was fully relaxed on the bottom electrode, the top electrode was pushed toward the bottom and then pressed the molecule with a constant speed. When the gap between the two electrodes reached 3.2 nm, the motion of the top electrode reversed to expand the gap to 3.8 nm. This process was cycled 3 times. Meanwhile, the force applied on Az was recorded and has been plotted as a function of time (F–t curve) as well as the gap distance (F–D curve) as shown in Fig. 7b and c, respectively. As shown in the F–t curve (Fig. 7b), when the gap distance between the two electrodes was reduced to 3.8 nm, Az was attracted and attached to the top electrode. Hereafter, the force exerted by Az increased linearly with the approaching between the two electrodes. However, at the moment when the motion of the top electrode reversed, the force dropped immediately and turned from compression to tension. Such a mechanical pattern can be explained by considering that Az exhibits viscoelasticity, which can be described with the constitutive relation $F = kx + c\dot{x}$, where F is the applied force, x is the deformation, k is the elastic stiffness, and c is the viscosity coefficient of Az. As stated by this viscoelastic constitutive relation, when the deforming direction of Az is reversed, the sign of viscous force $c\dot{x}$ will be reversed accordingly. As a result, a steep will appear in the F–t curve, which is consistent with the simulative result. The F–D curves (Fig. 7c) corresponding to the three cycles show a high degree of consistency, which confirms the mechanical stability of Az under cyclic loads and repeatability of the experiments. The change in conformational angles and bond angles of the protein backbone during the mechanical manipulation has also been analyzed (Fig. S4, ESI†). However, no obvious cycling feature can be observed. Thus the conductance change under cyclic loads is not the origin of the secondary structure but the global deformation of Az.

The influence of force on the electronic properties of Az is also studied by means of density functional theory (DFT) simulations. It is too resource consuming to carry out relaxation for introducing electrodes and calculations of the electron transmission rate in such a large system with 4608 atoms. Instead, we calculated the molecular orbitals under different loads to analyze the problem qualitatively. First, the structure files of Az under 2 nN force in both pressing and releasing were picked out from the first cycle in MD simulations, which are marked as states A and B, respectively (Fig. 7b). For both states, the isopotential surface of 20 orbitals within ±0.2 eV around the Fermi level was obtained using ATK,[38,39,44,45] among which 9 orbitals that are closest to the Fermi level have been shown in Fig. 7d. Generally, there are more delocalized orbitals in state B, the number is 18 out of 20, compared to 11 in structure A (Table 1). The isopotential surfaces have also been compared one by one according to the relative positions of the Fermi level. It is found that most orbitals in structure B are more delocalized than their corresponding opponent in structure A. Because the delocalization of the orbital is closely related to the conductance of the molecule, the above results validate that Az conductance

Table 1 Statistics of delocalized and localize orbitals of structures A and B

	Delocalized	Localized
State A	11	9
State B	18	2

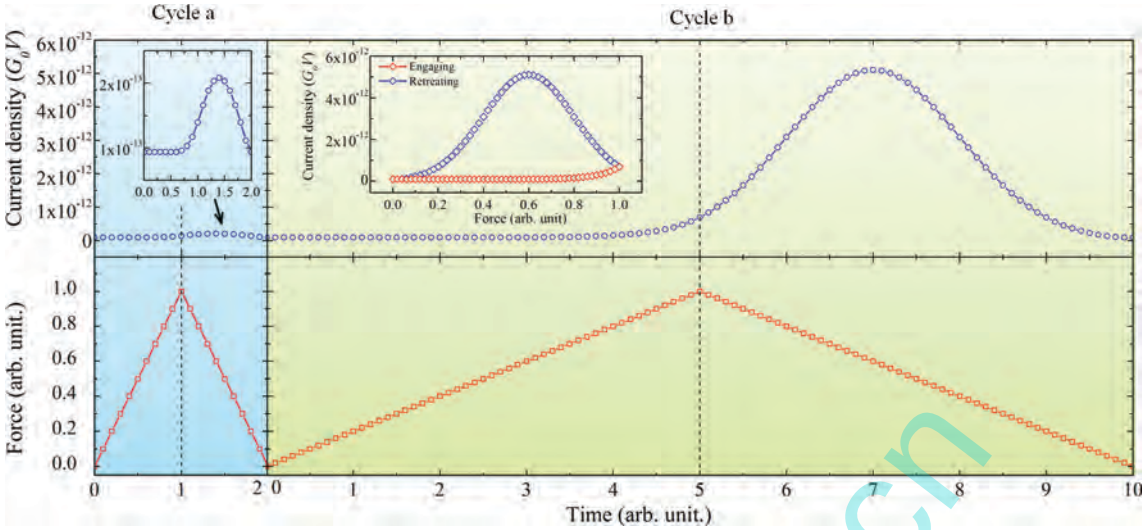

Fig. 8 The numerical calculation of I–t and F–t curves using the MMM model. The inset shows the current in cycle b as a function of force.

in releasing is higher than that in pressing under the same force magnitude. In addition, the energy spectrum in Fig. 7d shows that the gap between the HOMO and the LUMO in state A (A4 and A5) is obviously wider than that in state B (B5 and B6), which also agrees with the conclusion of orbital delocalization analysis.

Inspired by the experimental and simulative results, here we propose a phenomenological model to describe the MMM behavior. In the case of direct tunneling under small bias (*i.e.* ≤ 1 V), the current density through the Az monolayer can be expressed as $J(F, V, t) = G_0 \exp[-\lambda(F, t)]V$,[40,46,47] where G_0 is the reciprocal of effective contact resistance and $\lambda(F, t)$ is the structure-dependent factor reflecting the barrier height and width. According to the viscoelasticity shown by the results of MD simulations, the influence of force on the change rate of λ can be given by $\dot{\lambda}(F, t) = -\phi[F(t) - F_R]u(J - J_m)u(J_M - J)$, where ϕ is a constant associated with the viscosity coefficient of Az, u is the step function, which limits J within the permissible range (J_m, J_M), $F(t)$ is the pressing force and F_R is the restoring force determined by the deformation state of Az. This model states that, when $F(t) = F_R$, the structure of Az is at equilibrium, thus $\dot{\lambda} = 0$ and the conductance is stable. With $F(t) > F_R$, Az starts to creep and $\dot{\lambda} < 0$, which make the conductance increase over time. The case with $F(t) < F_R$ is just the opposite. A numerical calculation was carried out to estimate the current variation of Az described by this MMM model. As shown in Fig. 8, an arbitrary period cyclic load was first exerted on Az in cycle a, followed by cycle b with five times longer period. These two cycles have the same peak force F_M. For simplicity, F_R was chosen to be a constant as $F_R = 0.6F_M$. As for other parameters, the initial value of λ can be approximately given as $\lambda|_{t=0} = 30$ according to previous literature.[25,47] And $\phi = 5$ was found to work well in matching the experimental results. Current density obtained from the numerical calculation shows high consistency with our experimental results. Clear delayed peak current can be found in both cycles, and the peak value shows obvious period dependency, which validate our model for the MMM behavior of Az.

Conclusions

To summarize, the dynamic conductance response of the Az monolayer under cyclic loads has been revealed by a series of CAFM measurements under continuous cyclic loads. Nonlinear force dependency and delayed peak current have been observed in both I–Z measurements and I–t curves, which are significantly distinct from the characteristic of quasi-static results. The period and peak force of cyclic loads are found to have a great impact on the height of delayed peak current, showing that the conductance of the Az monolayer not only responds to the force magnitude but also dependent on the loading time. Generally, the dynamic variation of Az conductance is process-related and dominated by the time integral of force. In this work, this regular dynamic response of the Az conductance under mechanical force looks like a type of memristive behavior, which is defined as MMM behavior. By molecular dynamics and first-principles simulations, the MMM behavior has been further confirmed and expounded. A phenomenological model also clearly describes the MMM behavior of Az. The corresponding numerical results are in good agreement with our experimental data.

Since the origin of MMM behavior, viscoelasticity, is widely present in various proteins, this unique behavior may well be found in other proteins. Once it is confirmed, such property will certainly inspire new thought into related research field. On the one hand, this process-related electronic behavior of the proteins has great potential for building highly functional molecular devices such as molecular multi-state memory devices, force sensors, *etc.* On the other hand, previous studies have suggested that memristive behavior is connected to adaptation and even learning behavior of living organisms.[48] It is reasonable to expect that MMM behavior in proteins might be the

interpretation for adaptation and learning behavior under mechanical stimuli on the molecular scale. Nevertheless, the details are still needed for further investigation.

Acknowledgements

The authors gratefully acknowledge the financial support of the National Key Basic Research Program of China (No. 2015CB351905), NSFC (No. 11402312, 11474363, 11232015, and 11672339). Yue Zheng is also grateful for the support from Fok Ying Tung Foundation, Guangdong Natural Science Funds for Distinguished Young Scholar and China Scholarship Council.

Notes and references

1 C. Joachim, J. K. Gimzewski and A. Aviram, Electronics Using Hybrid-Molecular and Mono-Molecular Devices, *Nature*, 2000, **408**, 541–548.
2 M. A. Ratner, Brief History of Molecular Electronics, *Nat. Nanotechnol.*, 2013, **8**, 378–381.
3 N. J. Tao, Electron Transport in Molecular Junctions, *Nat. Nanotechnol.*, 2006, **1**, 173–181.
4 L. Sun, Y. A. Diaz-Fernandez, T. A. Gschneidtner, F. Westerlund, S. Lara-Avila and K. Moth-Poulsen, Single-Molecule Electronics: from Chemical Design to Functional Devices, *Chem. Soc. Rev.*, 2014, **43**, 7378–7411.
5 T. R. Prytkova, I. V. Kurnikov and D. N. Beratan, Coupling Coherence Distinguishes Structure Sensitivity in Protein Electron Transfer, *Science*, 2007, **315**, 622–625.
6 S. S. Skourtis and D. N. Beratan, Theories of Structure–Function Relationships for Bridge-Mediated Electron Transfer Reactions, *Adv. Chem. Phys.*, 1999, **106**, 377–452.
7 X. Y. Zhang, J. Shao, S. X. Jiang, B. Wang and Y. Zheng, Structure-Dependent Electrical Conductivity of Protein: Its Differences between Alpha-Domain and Beta-Domain Structures, *Nanotechnology*, 2015, **26**, 125702.
8 R. Rinaldi, A. Biasco, G. Maruccio, V. Arima, P. Visconti, R. Cingolani and M. P. Verbeet, Electronic Rectification In Protein Devices, *Appl. Phys. Lett.*, 2003, **82**, 472–474.
9 D. M. Cardamone and G. Kirczenow, Single-Molecule Device Prototypes for Protein-Based Nanoelectronics: Negative Differential Resistance and Current Rectification in Oligopeptides, *Phys. Rev. B: Condens. Matter Mater. Phys.*, 2008, **77**, 165403.
10 Y. Liu, H. L. Cai, M. Zelisko, Y. Wang, J. Sun, F. Yan, X. Meng, Y. Zhang and J. Li, Ferroelectric Switching of Elastin, *Proc. Natl. Acad. Sci. U. S. A.*, 2014, **111**, E2780–E2786.
11 J. Li, Y. Liu, Y. Zhang, H. L. Cai and R. G. Xiong, Molecular Ferroelectrics: Where Electronics Meet Biology, *Phys. Chem. Chem. Phys.*, 2013, **15**, 20786–20796.
12 C. I. Branden, *Introduction to Protein Structure*, Garland Science, 1999.
13 G. Bao, Mechanics of Biomolecules, *J. Mech. Phys. Solids*, 2002, **50**, 2237–2274.
14 X. Luo and J. J. Davis, Cheminform Abstract: Electrical Biosensors and the Label Free Detection of Protein Disease Biomarkers, *Chem. Soc. Rev.*, 2013, **42**, 5944–5962.
15 G. Zheng, F. Patolsky, Y. Cui, W. U. Wang and C. M. Lieber, Multiplexed Electrical Detection of Cancer Markers with Nanowire Sensor Arrays, *Nat. Biotechnol.*, 2005, **23**, 1294–1301.
16 L. Scullion, T. Doneux, L. Bouffier, D. G. Fernig, S. J. Higgins, D. Bethell and R. J. Nichols, Large Conductance Changes in Peptide Single Molecule Junctions Controlled by pH, *J. Phys. Chem. C*, 2011, **115**, 8361–8368.
17 E. A. Della Pia, M. Elliott, D. D. Jones and J. E. Macdonald, Orientation-Dependent Electron Transport in A Single Redox Protein, *ACS Nano*, 2011, **6**, 355–361.
18 J. M. Artés, I. Díez-Pérez and P. Gorostiza, Transistor-Like Behavior of Single Metalloprotein Junctions, *Nano Lett.*, 2011, **12**, 2679–2684.
19 I. Willner and E. Katz, Integration of Layered Redox Proteins and Conductive Supports for Bioelectronic Applications, *Angew. Chem., Int. Ed.*, 2000, **39**, 1180–1218.
20 B. Alberts, A. Johnson, J. Lewis, M. Raff, K. Roberts and P. Walter, *Mol. Biol. Cell*, Garland science, 5th edn, 2010.
21 A. W. Orr, B. P. Helmke, B. R. Blackman and M. A. Schwartz, Mechanisms of Mechanotransduction, *Dev. Cell*, 2006, **10**, 11–20.
22 F. X. Hart, The Mechanical Transduction of Physiological Strength Electric Fields, *Bioelectromagnetics*, 2008, **29**, 447–455.
23 J. Zhao and J. J. Davis, Force Dependent Metalloprotein Conductance by Conducting Atomic Force Microscopy, *J. Nanotechnol.*, 2003, **14**, 1023.
24 J. Zhao, J. J. Davis, M. S. Sansom and A. Hung, Exploring the Electronic and Mechanical Properties of Protein Using Conducting Atomic Force Microscopy, *J. Am. Chem. Soc.*, 2004, **126**, 5601–5609.
25 J. J. Davis, N. Wang, A. Morgan, T. Zhang and J. Zhao, Metalloprotein Tunnel Junctions: Compressional Modulation of Barrier Height and Transport Mechanism, *Faraday Discuss.*, 2006, **131**, 167–179.
26 W. Li, L. Sepunaru, N. Amdursky, S. R. Cohen, I. Pecht, M. Sheves and D. Cahen, Temperature and Force Dependence of Nanoscale Electron Transport *via* the Cu Protein Azurin, *ACS Nano*, 2012, **6**, 10816–10824.
27 L. D. Landau and E. M. Lifshitz, *Course of Theoretical Physics, Theory of elasticity*, 1986.
28 L. Chua, Memristor-the Missing Circuit Element, *IEEE Trans. Circuit Theory*, 1971, **18**, 507–519.
29 M. Di Ventra, Y. V. Pershin and L. O. Chua, Circuit Elements With Memory: Memristors, Memcapacitors, and Meminductors, *Proc. IEEE*, 2009, **97**, 1717–1724.
30 L. O. Chua and S. M. Kang, MemristiveDevices and Systems, *Proc. IEEE*, 1976, **64**, 209–223.
31 Y. Chen, G. Y. Jung, D. A. Ohlberg, X. Li, D. R. Stewart, J. O. Jeppesen and R. S. Williams, Nanoscale Molecular-Switch Crossbar Circuits, *Nanotechnology*, 2003, **14**, 462.
32 F. De Rienzo, R. R. Gabdoulline, M. C. Menziani and R. C. Wade, Blue Copper Proteins: A Comparative Analysis of Their Molecular Interaction Properties, *Protein Sci.*, 2000, **9**, 1439–1454.

33 E. Estrada and E. Uriarte, Folding Degrees Of Azurins and Pseudoazurins: Implications for Structure and Function, *Comput. Biol. Chem.*, 2005, **29**, 345–353.
34 A. D. MacKerell Jr, D. Bashford, M. L. D. R. Bellott, R. L. Dunbrack Jr, J. D. Evanseck, M. J. Field and D. Joseph-McCarthy, All-Atom Empirical Potential for Molecular Modeling and Dynamics Studies of Proteins, *J. Phys. Chem. B*, 1998, **102**, 3586–3616.
35 J. C. Phillips, R. Braun, W. Wang, J. Gumbart, E. Tajkhorshid, E. Villa and K. Schulten, Scalable molecular dynamics with NAMD, *J. Comput. Chem.*, 2005, **26**, 1781–1802.
36 L. W. Ungar, N. F. Scherer and G. A. Voth, Classical Molecular Dynamics Simulation of the Photo Induced Electron Transfer Dynamics of Plastocyanin, *Biophys. J.*, 1997, **72**, 5.
37 J. Feng, R. B. Pandey, R. J. Berry, B. L. Farmer, R. R. Naik and H. Heinz, Adsorption Mechanism of Single Amino Acid and Surfactant Molecules to Au{111} Surfaces in Aqueous Solution: Design Rules for Metal-Binding Molecules, *Soft Matter*, 2011, **7**, 2113–2120.
38 M. Brandbyge, J. L. Mozos, P. Ordejón, J. Taylor and K. Stokbro, Density-Functional Method for Nonequilibrium Electron Transport, *Phys. Rev. B: Condens. Matter Mater. Phys.*, 2002, **65**, 165401.
39 J. P. Perdew, K. Burke and M. Ernzerhof, Generalized Gradient Approximation Made Simple, *Phys. Rev. Lett.*, 1996, **77**, 3865.
40 X. D. Cui, A. Primak, X. Zarate, J. Tomfohr, O. F. Sankey, A. L. Moore and S. M. Lindsay, Reproducible Measurement of Single-molecule Conductivity, *Science*, 2001, **294**, 571–574.
41 F. Chen, J. Hihath, Z. Huang, X. Li and N. J. Tao, Measurement of single-Molecule Conductance, *Annu. Rev. Phys. Chem.*, 2007, **58**, 535–564.
42 Y. Xue, S. Datta and M. A. Ratner, Charge Transfer and "Band Lineup" in Molecular Electronic Devices: A Chemical and Numerical Interpretation, *J. Chem. Phys.*, 2001, **115**, 4292–4299.
43 S. Y. Quek, L. Venkataraman, H. J. Choi, S. G. Louie, M. S. Hybertsen and J. B. Neaton, Amine-Gold Linked Single-Molecule Circuits: Experiment and Theory, *Nano Lett.*, 2007, **7**, 3477–3482.
44 J. Shao, X. Y. Zhang, Y. Zheng, B. Wang and Y. Chen, Length-Dependent Rectification and Negative Differential Resistance in Heterometallic *n*-Alkanedithiol Junctions, *RSC Adv.*, 2015, **5**, 13917–13922.
45 J. Shao, X. Y. Zhang, Y. Chen and Y. Zheng, Charge Carrier Transition In an Ambipolar Single-Molecule Junction: Its Mechanical-Modulation and Reversibility, *npj Computational Materials*, 2016, **2**, 2.
46 D. J. Wold, R. Haag, M. A. Rampi and C. D. Frisbie, Distance Dependence of Electron Tunneling Through Self-Assembled Monolayers Measured by Conducting Probe Atomic Force Microscopy: Unsaturated Versus Saturated Molecular Junctions, *J. Phys. Chem. B*, 2002, **106**, 2813–2816.
47 *Nano and molecular electronics handbook*, ed. S. E. Lyshevski, CRC Press, 2016.
48 Y. V. Pershin, F. S. La and V. M. Di, Memristive Model of Amoeba Learning, *Phys. Rev. E: Stat., Nonlinear, Soft Matter Phys.*, 2009, **80**, 301–327.